

Progress and Research Issues in High-Frequency Seafloor Scattering

Darrell R. Jackson

Applied Physics Laboratory, University of Washington, Seattle, WA 98105

Abstract. The status of model-data comparisons for seafloor scattering is reviewed. The small-roughness perturbation and small-slope approximations have proven accurate and useful in treating scattering by interface roughness, and have been extended from the fluid case to the elastic and poroelastic cases. The problem of scattering by sediment heterogeneity is more difficult, but the method of small perturbations has been tested successfully in several experiments. Further tests are needed, particularly with respect to scattering by discrete inclusions. Stratification has been modeled in both roughness and volume scattering, but only a few experimental tests have been attempted.

INTRODUCTION

Substantial progress has been made in recent years toward understanding and modeling the physical processes responsible for acoustic scattering by the seafloor. This has been possible due to the increasing effort devoted to characterization of the sediment physical parameters that control scattering. Seafloor scattering is most often described in terms of the scattering cross section per unit area per unit solid angle or its decibel equivalent, scattering strength. In most modeling approaches, the cross section is assumed to be a sum of two terms, one representing scattering due to interface roughness and the other representing scattering due to volume heterogeneity of the sediment. This idealization is avoided in some recent work [1].

SCATTERING BY INTERFACE ROUGHNESS

The two most commonly used approximations for scattering by seafloor roughness are the small-roughness perturbation method (sometimes known as Rayleigh-Rice perturbation theory) and the Kirchhoff approximation (also known as the tangent-plane approximation). Each has its own separate domain of validity, with perturbation theory tending to be most accurate for scattering at wide angles relative to the specular (flat-interface reflection) direction and the Kirchhoff approximation being better for scattering near the specular direction. The small-slope approximation [2, 3] provides some of the best properties of the two in a logical expansion scheme.

The small-perturbation, Kirchhoff, and small-slope approximations yield equations whose general form does not depend upon the particular wave theory employed. That is, these forms are the same whether the sediment is modeled as a fluid, a viscoelastic solid or a poroelastic medium. The general forms for the bistatic scattering cross-section in these

three scattering approximations are, in the small-roughness perturbation approximation:

$$\sigma = k_w^4 |A|^2 W_2(\Delta \mathbf{K}) , \quad (1)$$

in the Kirchhoff approximation:

$$\sigma = \frac{|V(\theta_{is})|^2}{8\pi} \left[\frac{\Delta k^2}{\Delta K \Delta k_z} \right]^2 I_K , \quad (2)$$

and, in the small-slope approximation:

$$\sigma = \frac{k_w^4 |A|^2}{2\pi \Delta K^2 \Delta k_z^2} I_K . \quad (3)$$

The wavenumber in water is denoted k_w , and the argument, Δk , appearing in Equation (2), is the magnitude of the difference of the scattered and incident wave vectors. Similarly, $\Delta \mathbf{K}$, is the horizontal component of this difference, the so-called ‘‘Bragg wave vector’’. The magnitude of this difference is denoted ΔK and appears in Equations (2) and (3) along with the vertical component of the difference, Δk_z . These variables are related by $\Delta k^2 = \Delta K^2 + \Delta k_z^2$. The ‘‘Kirchhoff integral’’

$$I_K = \frac{\Delta K^2}{2\pi} \int e^{-i\Delta \mathbf{K} \cdot \mathbf{R}} [e^{-\frac{1}{2}\Delta k_z^2 S(\mathbf{R})} - e^{-\Delta k_z^2 h^2}] d^2 R \quad (4)$$

does not depend upon the choice of wave theory and is common to both the Kirchhoff and small-slope approximations. The spectrum, $W_2(\Delta \mathbf{K})$, appearing in the small-roughness cross-section and the structure function, $S(\mathbf{R})$, appearing in the Kirchhoff integral are related by a transform, so that knowledge of one is sufficient to determine the other. The factor A depends upon choice of wave theory, but is common to both the perturbation and small-slope approximations. The reflection coefficient, V , appearing in the Kirchhoff expression depends upon the choice of wave theory, and is evaluated at the grazing angle

$$\theta_{is} = \sin^{-1} \left(\frac{\Delta k}{2k_w} \right) \quad (5)$$

that corresponds to specular reflection from the source to the receiver with the rough surface tilted in such a way as to provide such a reflection.

In summary, a particular wave theory must be applied to obtain A for small-roughness perturbation and small-slope approximations or, correspondingly, V for the Kirchhoff approximation. Once these theoretical tasks are complete, only numerical computation remains, including evaluation of Equation (4) [4].

Attention will be focused on the small-roughness perturbation approach, as it is applicable over a wide range of angles, excluding near-specular directions. In addition, its predictions are essentially the same as those of the small-slope approximation in this angular range for typical seafloor parameters. The simplest and most widely used model treats the sediment as a fluid. In this case, the factor A in (1) and (3) is given by [11]

$$A = \frac{1}{2} [1 + V(\theta_i)][1 + V(\theta_s)] G , \quad (6)$$

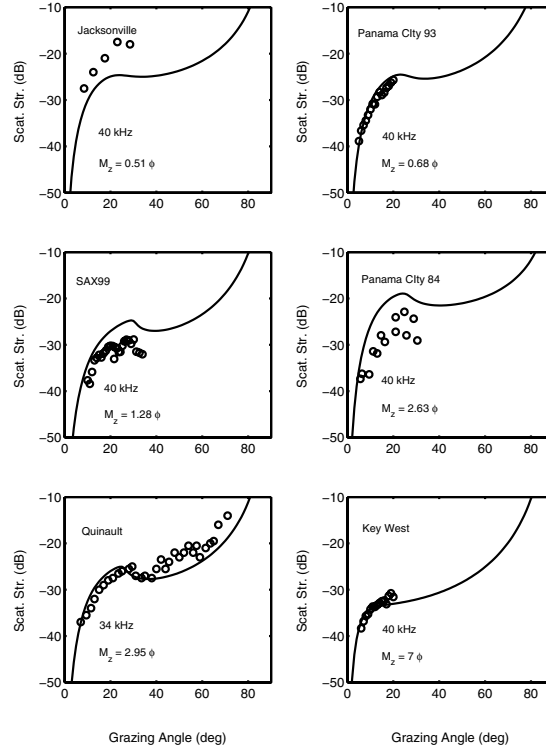


FIGURE 1. Comparison of fluid small-roughness perturbation model with data from six experiments conducted at sandy sites. The examples are given in order of increasing grain size, M_z , and the primary acoustic and geoaoustic data sources are: Jacksonville [5], Panama City 93 [6], SAX99 [7], Panama City 84 [8], Quinault [9], and Key West [10].

where

$$G = (1/a_\rho - 1) \left[\cos \theta_i \cos \theta_s \cos \phi_s - \frac{\sin \theta_{pi} \sin \theta_{ps}}{a_p^2 a_\rho} \right] + 1 - \frac{1}{a_p^2 a_\rho}, \quad (7)$$

and

$$\sin \theta_{pi} = \sqrt{1 - a_p^2 \cos^2 \theta_i}, \quad (8)$$

$$\sin \theta_{ps} = \sqrt{1 - a_p^2 \cos^2 \theta_s}. \quad (9)$$

In these expressions, θ_i and θ_s are the incident and scattered grazing angles, ϕ_s is the “bistatic angle,” equal to zero in the specular direction and equal to π in the backscattering direction. The ratio of sediment mass density to water mass density is denoted a_ρ , and a_p is the corresponding (complex) ratio for compressional wave speeds.

Figure 1 compares the small-roughness, fluid-sediment model with data from six experiments conducted at sandy sites. The fit between the model and data appears to be reasonably good, with the greatest model-data difference occurring for the two intermediate grain size cases, SAX99 and Panama City 84. A detailed error analysis has been performed for the SAX99 data [7], with the conclusion that the model-data

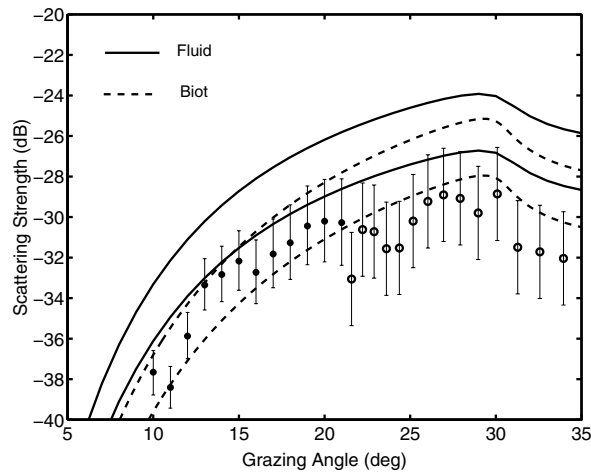


FIGURE 2. Comparison of measured bottom backscattering strength at 40 kHz with small-roughness perturbation fluid model (solid curves) and Biot model (dashed curves). The upper and lower curves in each case give the 95% uncertainty bounds for the models based on the uncertainty bounds for the roughness data. The vertical error bars give the corresponding 95% uncertainty bounds for the acoustic measurements. The data denoted by filled circles were taken at the same site as the roughness measurements, whereas the data denoted by open circles were obtained using a different apparatus at a site removed by a few hundred meters. The slight offset between these data sets may be due to either acoustic calibration error, difference in roughness at the two sites, or a combination of these two. (Figure adapted from [7])

difference is significant and likely due to neglect of poroelastic (Biot) effects. The similar model-data differences seen at the Panama City 84 site [8] may be due to the same cause. One significant point of agreement between model and data is the scattering strength maximum occurring near the critical angle, visible in the data from SAX99, Panama City 84, and Quinault. No maximum is predicted or seen for the finer grain sediment of the Key West site.

The Biot model has been compared with backscattering strength data in [7]. Figure 2 shows that, within the uncertainties of acoustic measurement and the uncertainties in model inputs, the Biot model provides a better fit to the data than the fluid model. A nearly identical fit would be provided by the “effective density” approximation [12] in which the sediment is modeled as a fluid having a reduced value of density, this value being computed in terms of a few of the Biot parameters.

Roughness scattering by viscoelastic seafloors has been treated in the perturbation [13, 14] and small-slope [15, 16, 17] approximations. Shear effects are negligible for sandy seafloors [18], but significant for rock seafloors. Testing of available models at well-characterized rocky sites presents a difficult challenge.

Gradients in sediment physical properties can influence scattering owing to the incidence of energy from below the sediment-water interface. Ivakin has developed a general formalism [1] that lends itself to layered seafloors, including cases where the distinction between roughness and volume scattering is not clear. Less generally, one may simply include the upward reflected wave in the perturbation treatment [10]. This leads to the relatively simple result presented in Equation (6) in which the effect of the energy inci-

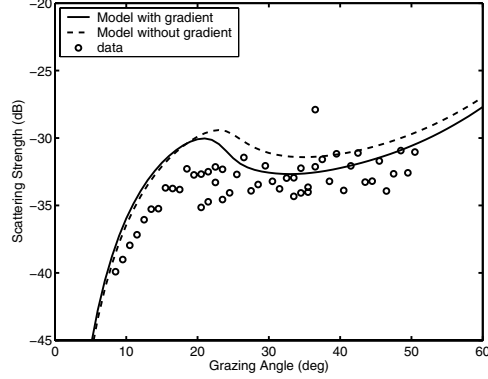


FIGURE 3. Effect of gradients in roughness scattering model using acoustic and geoacoustic data from [19]. The frequency is 140 kHz and the seafloor is a silty sand. Gradients are treated using Equation (6).

dent from below is contained in the reflection coefficient, V , which must be computed including the effects of stratification. In the measurements reported by Pouliquen and Lyons [19], gradients had a significant effect, and the inclusion of gradient effects via a numerically computed reflection coefficient improves the model-data fit, as shown in Fig. 3.

SCATTERING BY VOLUME HETEROGENEITY

As with roughness scattering, attention will be focused on the method of small perturbations as applied to sediment volume scattering. It is in this arena that the most rigorous model-data comparisons have been made. If the sediment is treated as a fluid, an effective interface bistatic cross section can be defined as follows:

$$\sigma = \frac{|[1 + V(\theta_i)][1 + V(\theta_s)]|^2 \sigma_v}{2\alpha_\rho^2 \Im[k_p(\sin \theta_{pi} + \sin \theta_{ps})]}, \quad (10)$$

where the volume scattering cross section per unit solid angle per unit volume is

$$\sigma_v = \frac{\pi |k_p|^4}{2} \left[W_{\kappa\kappa}(\Delta \mathbf{k}_p) + 2\Re \left\{ \frac{\mathbf{k}_{ps} \cdot \mathbf{k}_{pi} k_p^{*2}}{|k_p|^4} W_{\rho\kappa}(\Delta \mathbf{k}_p) \right\} + \frac{|\mathbf{k}_{ps} \cdot \mathbf{k}_{pi}|^2}{|k_p|^4} W_{\rho\rho}(\Delta \mathbf{k}_p) \right]. \quad (11)$$

The wavenumber for compressional waves in the sediment is $k_p = k_w/a_p$, and the function $W_{\kappa\kappa}$ is the three-dimensional spectrum for the fluctuations in normalized sediment compressibility. The normalization consists in dividing the fluctuating part of the compressibility (which is the inverse of the bulk modulus) by the mean compressibility. Similarly, $W_{\rho\rho}$ is the spectrum for normalized density fluctuations, and $W_{\rho\kappa}$ is the cross-spectrum that expresses the correlation between these two random variables.

The wave vectors, \mathbf{k}_{pi} and \mathbf{k}_{ps} , for the incident and scattered compressional waves in the sediment have the same horizontal components as the corresponding wave vectors in

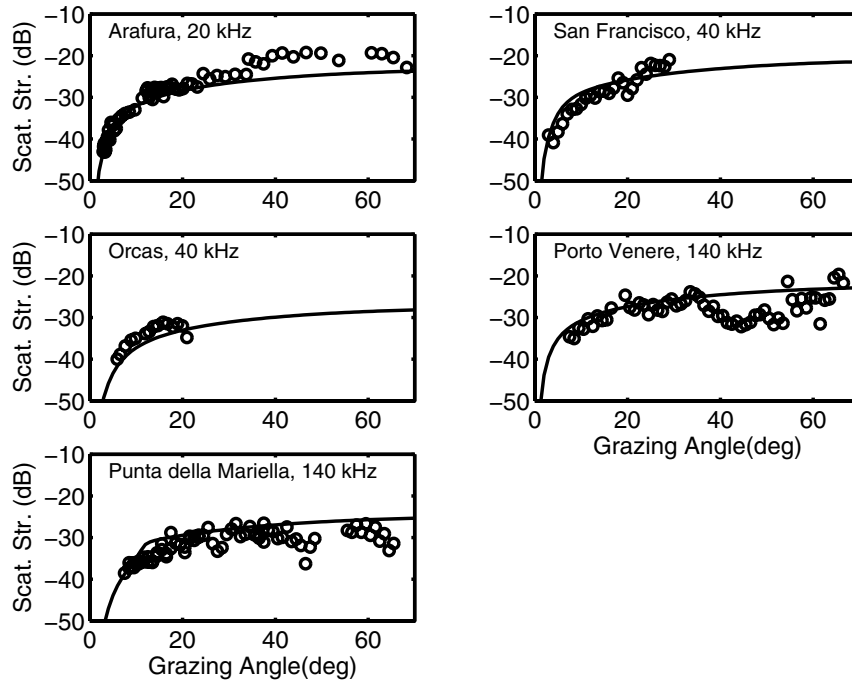


FIGURE 4. Comparison of the fluid volume scattering perturbation model with backscattering strength measured at five sites having soft sediments. The primary acoustic and geoacoustic data sources are: Arafura [9], San Francisco [9], Orcas [20], Porto Venere [19], Punta della Mariella [19]. The volume heterogeneity parameters for the Arafura and San Francisco sites were taken from [21].

water and complex z-components determined by Equations (8) and (9). The spectra in Equation (11) are evaluated at the Bragg wave vector, $\Delta\mathbf{k}_p$:

$$\Delta\mathbf{k}_p = \Re\{\mathbf{k}_{ps} - \mathbf{k}_{pi}\}. \quad (12)$$

The Bragg wave vector is the real part of the wave vector difference. If the complex difference were required instead, one would be faced with the issue of analytic continuation of the spectrum to complex arguments. This issue cannot be avoided when treating volume scattering in elastic or layered media.

Figure 4 compares higher-frequency backscattering data obtained by several different investigators with the perturbation model. These model-data comparisons are the same, except for details, as those given in the primary references. The model-data agreement is satisfactory, but some of the comparisons are not as rigorous as one might wish. In particular, the volume heterogeneity data for the Arafura, San Francisco, and Orcas sites were obtained from small-diameter, short core samples and were analyzed in the vertical coordinate only. The three-dimensional spectra were assumed to be isotropic. The Arafura site had a large concentration of buried shell fragments, calling into question the use of the perturbation approach. In all cases, the density–compressibility cross spectrum was not determined by measurement, but assigned a default value.

Further effort is required to obtain accurate estimates of sediment heterogeneity statistics. Nevertheless, the results of these model-data comparisons are encouraging and indicate that the perturbation model for sediment volume scattering is a reasonable approximation in many cases of interest.

Corresponding perturbation expressions are available for volume scattering in viscoelastic material, [22, 14, 18], but have not been tested experimentally. The poroelastic volume scattering problem has been treated in the perturbation approximation [23], but results are not yet available in a form appropriate to the high-frequency seafloor problem.

REFERENCES

1. Ivakin, A., *J. Acoust. Soc. Am.*, **103**, 827–837 (1998).
2. Voronovich, A., *Soc. Phys. J. ETP*, **62**, 65–70 (1985).
3. Thorsos, E., and Broschat, S., *J. Acoust. Soc. Am.*, **97**, 2080–2093 (1995).
4. Drumheller, D., and Gragg, R., *J. Acoust. Soc. Am.*, **110**, 2270–2275 (2001).
5. Stanic, S., Briggs, K., Fleischer, P., Sawyer, W. B., and Ray, R., *J. Acoust. Soc. Am.*, **85**, 125–136 (1989).
6. Jackson, D., Briggs, K., Williams, K., and Richardson, M., *IEEE J. Oceanic Engr.*, **21**, 458–470 (1996).
7. Williams, K., Jackson, D., Thorsos, E., Tang, D., and Briggs, K., *IEEE J. Oceanic Engr.*, **27**, 376–387 (2002).
8. Stanic, S., Briggs, K., Fleischer, P., Ray, R., and Sawyer, W., *J. Acoust. Soc. Am.*, **83**, 2134–2144 (1988).
9. Jackson, D., and Briggs, K., *J. Acoust. Soc. Am.*, **92**, 962–977 (1992).
10. Briggs, K., Williams, K., Jackson, D., Jones, C., Ivakin, A., and Orsi, T., *Marine Geology*, **182**, 141–159 (2002).
11. Moe, J., and Jackson, D., *J. Acoust. Soc. Am.*, **96**, 1748–1754 (1994).
12. Williams, K., *J. Acoust. Soc. Am.*, **110**, 2956–2963 (2001).
13. Essen, H., *J. Acoust. Soc. Am.*, **95**, 1299–1301 (1994).
14. Jackson, D., and Ivakin, A., *J. Acoust. Soc. Am.*, **103**, 336–345 (1998).
15. Yang, T., and Broschat, S., *J. Acoust. Soc. Am.*, **96**, 1796–1803 (1994).
16. Gragg, R., Wurmser, D., and Gauss, R., *J. Acoust. Soc. Am.*, **110**, 2878–2901 (2001).
17. Soukoup, R., and Gragg, R., *J. Acoust. Soc. Am.*, **113**, 2501–2514 (2003).
18. Ivakin, A., and Jackson, D., *J. Acoust. Soc. Am.*, **103**, 346–354 (1998).
19. Pouliquen, E., and Lyons, A., *IEEE J. Oceanic Eng.*, **27**, 388–402 (2002).
20. Jones, C., and Jackson, D., “Temporal Fluctuations of Backscattered Field Due to Bioturbation in Marine Sediments,” in *High Frequency Acoustics in Shallow Water*, edited by N. Pace, E. Pouliquen, O. Bergem, and A. Lyons, NATO SACLANT Undersea Res. Ctr., La Spezia, Italy, 1997, pp. 275–282.
21. Yamamoto, T., *J. Acoust. Soc. Am.*, **99**, 866–879 (1996).
22. Ivakin, A., *Soviet Physics–Acoust.*, **36**, 377–380 (1990).
23. Gurevich, B., Sadovnichaja, A., Lopatnikov, S., and Shapiro, S. A., *Geophys. J. Int.*, **133**, 91–103 (1998).